

Observation of the fractional ac Josephson effect: the signature of Majorana particles

Leonid P. Rokhinson,^{1,2,*} Xinyu Liu,³ and Jacek K. Furdyna³

¹*Department of Physics, Purdue University, West Lafayette, Indiana 47907 USA*

²*Birck Nanotechnology Center, Purdue University, West Lafayette, Indiana 47907 USA*

³*Department of Physics, University of Notre Dame, Notre Dame, Indiana 46556 USA*

(Dated: Submitted to Science on March 20, 2012)

We report the observation of the fractional ac Josephson effect in hybrid semiconductor/superconductor InSb/Nb nanowire junctions, a hallmark of topological matter. When the junction is irradiated with rf frequency f_0 at zero external magnetic field, quantized voltage steps (Shapiro steps) with a height $\Delta V = hf_0/2e$ are observed, as is expected for conventional superconductor junctions where the supercurrent is carried by charge- $2e$ Cooper pairs. At high fields the height of the first Shapiro step is doubled to hf_0/e . The supercurrent carried by charge- e quasiparticles is a unique signature of Majorana fermions, elusive particles predicted *ca.* 80 years ago.

In 1928 Dirac reconciled quantum mechanics and special relativity in a set of coupled equations which became the cornerstone of quantum mechanics[1]. Its main prediction that every elementary particle has a complex conjugate counterpart – an antiparticle – has been confirmed by numerous experiments. However, even at the dawn of quantum mechanics some physicists were not satisfied with the notion that elementary particles are described by complex wavefunctions. In 1937 Majorana showed how Dirac’s equation for spin-1/2 particles can be modified to permit real wavefunctions[2, 3]. However, the complex conjugate of a real number is the number itself, which means that such particles are their own antiparticles. Majorana hypothesized that the neutrino may be such a particle, and the search for so-called “sterile” massless neutrinos is still ongoing[4].

The most intriguing feature of Majorana particles is that in low dimensions they obey non-Abelian statistics. The revival of current interest in Majorana particles started with a seminal paper by Kitaev[5], who showed theoretically that quasiparticles with non-Abelian statistics can be used to realize quantum gates that are topologically protected from local sources of decoherence. While Majorana fermions seem to be absent from the world of elementary particles, excitations sharing their properties may emerge in electronic systems. It has been predicted that Majorana excitations may be formed in some unconventional states of matter, including certain fractional quantum Hall effect states[6], chiral p -wave superconductors[7], superfluids with order parameter $p_x + ip_y$ symmetry[8], in hybrid topological insulator/superconductor structures[9], and semiconductor/superconductor structures[10–12].

Ordinary spin-1/2 particles or excitations carry a charge, and thus cannot be their own antiparticles. In a superconductor, however, free charges are screened, and charge-less spin-1/2 excitations become possible. BCS theory allows fermionic excitations which are a mixture of electron and hole creation operators, $\gamma_i = c_i^\dagger + c_i$. This creation operator is invariant with respect to charge conjugation, $c_i^\dagger \leftrightarrow c_i$. If the energy of an excitation created in this way is

* To whom correspondence should be addressed. E-mail: leonid@purdue.edu

zero, the excitation will be a Majorana particle. However, zero modes are not permitted in ordinary s -wave superconductors.

The current work is inspired by the paper of Sau *et al.* [10] who predicted that Majorana fermions can be formed in a coupled semiconductor/superconductor system. Superconductivity can be induced in a semiconductor material by the proximity effect. At zero magnetic field electronic states are doubly-degenerate and Majorana modes are not supported. If the semiconductor has strong spin-orbit (SO) interactions, the two spin branches will be separated in momentum space, but the SO interactions do not lift the Kramer's degeneracy. However, in a magnetic field $\mathbf{B} \perp \mathbf{B}_{\text{so}}$ there is a range of energies where a single mode is crossing the Fermi energy[13]. Proximity effect in this regime may drive the system into a topological superconducting state which supports Majorana modes. Theoretically, it has been predicted that proper conditions for this to occur can be realized in 2D [10, 14] and 1D systems[11, 12]. Moreover, multiband nanowires should also support topological superconductivity[15, 16].

What are the experimental signatures of Majorana particles? Majorana modes come in pairs, and zero energy Andreev end-modes localized at the ends of a wire can be probed in tunneling experiments[17–19]. There are some reports of zero bias anomaly observed in topological insulator/superconductor structures[20]. However, conductivity enhancement near zero bias is also a signature of diverse phenomena in mesoscopic physics, such as the Kondo effect in quantum dots[21] or the “0.7 anomaly” in nanowires[22]. Superposition of two Majorana modes constitutes an ordinary fermion; and, uniquely to Majorana particles, interference with charge- e (Majorana) rather than charge- $2e$ (Cooper pairs) periodicity modifies the Josephson relation[5, 11, 23, 24]. In the dc Josephson effect, fluctuations between filled and empty Majorana modes will mask the charge- e periodicity and, indeed, we observe $2e$ periodicity with multiple phase slips in a dc SQUID configuration. In the ac Josephson effect the charge- e periodicity due to Majorana modes is fully revealed.

The devices were fabricated from undoped $\text{In}_{0.6}\text{Ga}_{0.4}\text{Sb}/\text{InSb}/\text{In}_{0.6}\text{Ga}_{0.4}\text{Sb}$ 3nm/20nm/3nm quantum wells grown by molecular beam epitaxy on n-doped (001) GaSb substrates. A thick graded $\text{In}_x\text{Ga}_{1-x}\text{Sb}$ ($x = .17 - .6$) buffer and a 120nm $\text{In}_{0.77}\text{Al}_{0.33}\text{Sb}$ barrier were grown between the wafer and the quantum well for strain relaxation and electron confinement. A pattern of multiple Josephson junctions (JJs) were defined by e-beam lithography, and 45 nm of Nb were deposited by dc sputtering. A large scale image and an AFM micrograph of a JJ region are shown in Fig. 1. The actual JJ is formed between two 120 nm-wide and 1 μm -long Nb wires. Each device consists of two JJs with nominally the same gaps connected in parallel in a dc SQUID geometry. Each sample has several such devices, with gaps ranging between 40-120 nm. During Nb deposition a thin (2-3 nm) layer of Nb is formed, extending 70-80 nm outside the pattern. This layer can be seen on the AFM image as a brown halo around the wire. This thin layer is used as an etch mask to define the nanowire in the underlying semiconductor. Etching in $\text{H}_2\text{SO}_4:\text{H}_2\text{O}_2:\text{H}_2\text{O}$ 1:8:1000 for 30 sec removes 60 nm of the semiconductor, and thus a continuous ≈ 290 nm-wide InSb wire is formed under the Nb. The wires are wide and thin, and spin-orbit interactions are dominated by the Dresselhaus term $H_D = \gamma_D \langle k_z^2 \rangle (k_x \sigma_x - k_y \sigma_y)$, where $\langle k_z^2 \rangle = (\pi/d)^2$, $d = 20$ nm is the quantum well thickness, σ_i are Pauli matrices, \hat{x} , and \hat{y} are the principal crystallographic axes. The wires are oriented along the [110] crystallographic direction and the effective spin-orbit magnetic field $\mathbf{B}_{\text{so}} \perp \mathbf{I}$, as indicated by the green arrow on the AFM image. This configuration allows the formation of a pair of Majorana particles localized on each wire, one particle being localized at the end of the nanowire close to the JJ and the other one

localized at the end where the wire joins the wide region in which the condition $\mathbf{B}_{\text{so}} \perp \mathbf{I}$ is not satisfied.

As devices are cooled down, a series of superconducting transitions $T_{c1} - T_{c3}$ is observed (Fig. 2a). The first transition, $T_{c1} \sim 6.4$ K, is for wide areas and is close to the bulk $T_c^{\text{Nb}} = 9.3$ K; $T_{c2} = 5.8$ K is for the 120 nm-wide Nb wires; and $T_{c3} \approx 1.2$ K is for the JJs. A typical $V(I)$ characteristic of a device measured at the base temperature of 20 mK exhibits a clear supercurrent region ($V = 0$) with a hysteretic abrupt appearance of a finite voltage, characteristic of an underdamped capacitively shunted JJ[25]. The capacitance is formed between Nb wires and the doped GaSb substrate. The measured critical current $I_c = 0.3 - 5 \mu\text{A}$ in different devices is divided between two JJs connected in parallel. The ratio of critical currents in the two junctions, $r = I_{c1}/I_{c2}$, can be estimated by measuring the amplitude of voltage modulation $V \propto \sqrt{r^2 + 2r \cos(2\pi S B_{\perp}/\phi_0)}$ when a device is operated as a dc SQUID[26]. Here $\phi_0 = h/2e$ is the flux quantum, S is the area of the SQUID, and B_{\perp} is applied perpendicular to the surface. For the device characterized in Fig. 2 $r = 7.3$ and the current is dominated by one of the junctions. The normal resistance for this device is $R_N = 650 \Omega$, and the product $R_N I_c \approx 0.2$ mV. This value is close to the superconducting gap $\Delta/e = 1.8 k_B T_c = 0.18$ mV, indicative of a diffusive regime.

Normalized differential conductance, plotted in Fig. 2b, shows clear enhancement at low voltages. This excess current is a clear signature of Andreev reflection[27, 28]. Most important for our measurements is that the excess current, and thus coherent electron transport, is observed at high in-plane magnetic fields up to 4 T, as shown in the inset.

When samples are subjected to an external microwave field with the frequency f_0 , a phase locking between the rf field and the Josephson supercurrent gives rise to constant-voltage Shapiro steps[29] in the $V(I)$ characteristics at $V_n = nhf_0/q$, where h is Planck's constant, q is the charge of quasiparticles, and $n = 0, \pm 1, \pm 2, \dots$. A set of curves taken at different rf amplitudes V_{rf} is shown in Fig. 3. At $B = 0$ up to 4 steps with the height $6 \mu\text{V}$ are observed at $f_0 = 3$ GHz, consistent with the Cooper pair tunneling ($q = 2e$). The step height scales linearly with f_0 .

When in-plane magnetic field $\mathbf{B} \parallel \mathbf{I}$ is applied, Shapiro steps at $V = 6, 12$ and $18 \mu\text{V}$ are clearly visible at low fields, $B < 2.5$ T. Steps at 12 and $18 \mu\text{V}$ remain visible up to $B \approx 3.5$ T, while the step at $6 \mu\text{V}$ disappears above $B \approx 2.5$ T. Disappearance of all steps above 3.5 T is consistent with suppression of the excess current and Andreev reflection at high fields.

Quantitative comparison of the width of the Shapiro steps $\Delta I_n(V_{rf})$ for $n = 0, 1, 2$ and 3 is plotted in Fig. 4. At low fields the n -th step width ΔI_n is expected to follow a Bessel function dependence $\Delta I_n \propto |J_n(\beta V_{rf})|$, where $\beta = \alpha q / h \nu_{rf}$ and α is the rf amplitude attenuation. At $B = 0$ the $n = 0$ step vanishes at $V_{rf} = 5.8$ mV and re-appears at higher rf powers, allowing accurate determination of $\beta = 0.42 \text{ mV}^{-1}$. The same β is used to plot the expected dependence of ΔI_n for $n = 1, 2$ and 3, albeit with 8 times smaller pre-factor (the width of the $n = 0$ step is affected by large I_c in our samples). At high rf powers $V_{rf} > 8$ mV all steps disappear, presumably due to sample heating.

At $B = 2$ T the same $\beta = 0.42 \text{ mV}^{-1}$ fits the V_{rf} dependence of the $n = 0$ step and is qualitatively consistent with the evolution of $n = 1, 2$ and 3 steps. The maximum values of ΔI_1 and ΔI_2 reach ≈ 50 nA, and ΔI_3 reaches ≈ 30 nA. At $B = 2.7$ T ΔI_2 and ΔI_3 reach 46 and 23 nA, respectively, similar to the respective values at lower fields. At the same time the $V = 6 \mu\text{V}$ step almost disappears at $B = 2.7$ T ($\Delta I_1 < 4$ nA) and completely disappears at $B = 3$ T. Also, $\beta = 0.42 \text{ mV}^{-1}$ (solid line) does not provide a good fit to the evolution of the $n = 0$ plateau. The best fit is obtained with $\beta = 0.32 \text{ mV}^{-1}$ (dashed line).

The doubling of the Shapiro step height and the decrease of β are unique signatures of a topological quantum phase transition. At low magnetic fields states at the Fermi energy are doubly-degenerate as long as disorder δE and/or Fermi energy E_F in the wire are larger than the Zeeman gap $E_Z = g^* \mu_B B$. At high fields $E_Z > \delta E, E_F$, the energy spectrum in InSb nanowires becomes non-degenerate at the Fermi energy, and Andreev end-modes are supported as long as $E_{so} \gtrsim E_Z$ [10]. In this regime the supercurrent is carried by charge- e quasiparticles, and the height of the Shapiro steps should double on the non-trivial (high- B) side of the topological phase transition as $q = 2e$ becomes $q = e$. At the same time we expect β to be reduced by a factor of 2. Experimentally we see the doubling of the first Shapiro step from 6 to 12 μV . Also at high fields the width of the step at 12 μV is better described by $|J_1|$ rather than $|J_2|$ dependence, confirming that the step at 12 μV becomes the $n = 1$ step. The step at $V = 18 \mu\text{V}$ is observed up to the highest fields $B \approx 3.5 \text{ T}$, which may indicate finite probability of Cooper pair tunneling at high voltages. The coefficient β is reduced by 30% across the transition, although at high fields the measured β is most likely overestimated due to the suppression of all steps at $V_{rf} > 8 \text{ mV}$.

In this paper we report the observation of the fractional ac Josephson effect in InSb/Nb nanowires, strong experimental evidence that a topologically non-trivial superconducting state is formed in this system[11]. An important benefit of the semiconductor/superconductor system is that the device can be tuned across the topological phase transition by an external magnetic field, and properties of the topological and ordinary superconducting state can be compared for the same sample. The observed change of the Shapiro steps height and width is qualitatively consistent with the sample undergoing a topological phase transition as a function of B at $B \approx 2.5 \text{ T}$.

Acknowledgements The work was partially supported by ARO grant 56447-PH-QC (LR) and by NSF grant DMR10-05851 (JKF, XL). LR benefited from discussions with Roman Lutchyn.

-
- [1] P. A. M. Dirac, “The quantum theory of the electron,” *Proc. R. Soc. Lond. A* **117**, 610–624 (1928).
 - [2] E. Majorana, “Symmetrical theory of electrons and positrons,” *Nuovo Cimento* **14**, 171 – 184 (1937).
 - [3] Frank Wilczek, “Majorana returns,” *Nat Phys* **5**, 614–618 (2009).
 - [4] Adrian Cho, “The sterile neutrino: Fertile concept or dead end?” *Science* **334**, 304–306 (2011).
 - [5] A Yu Kitaev, “Unpaired Majorana fermions in quantum wires,” *Physics-Uspekhi* **44**, 131 (2001).
 - [6] G Moore and N Read, “Nonabelions in the fractional quantum Hall effect,” *Nuc. Phys. B* **360**, 362–396 (1991).
 - [7] Sankar Das Sarma, Chetan Nayak, and Sumanta Tewari, “Proposal to stabilize and detect half-quantum vortices in strontium ruthenate thin films: Non-abelian braiding statistics of vortices in a $p_x + ip_y$ superconductor,” *Phys. Rev. B* **73**, 220502 (2006).
 - [8] N. Read and D. Green, “Paired states of fermions in two dimensions with breaking of parity and time-reversal symmetries and the fractional quantum Hall effect,” *Phys. Rev. B* **61**, 10267–10297 (2000).
 - [9] Liang Fu and C.L. Kane, “Superconducting proximity effect and Majorana fermions at the

- surface of a topological insulator,” *Physical Review Letters* **100**, 096407 (2008).
- [10] J.D. Sau, R.M. Lutchyn, S. Tewari, and S. Das Sarma, “Generic new platform for topological quantum computation using semiconductor heterostructures,” *Physical Review Letters* **104**, 040502 (2010).
 - [11] Roman M. Lutchyn, Jay D. Sau, and S. Das Sarma, “Majorana fermions and a topological phase transition in semiconductor-superconductor heterostructures,” *Phys. Rev. Lett.* **105**, 077001 (2010).
 - [12] Yuval Oreg, Gil Refael, and Felix von Oppen, “Helical liquids and Majorana bound states in quantum wires,” *Phys. Rev. Lett.* **105**, 177002 (2010).
 - [13] C.H.L. Quay, T.L. Hughes, J.A. Sulpizio, L.N. Pfeiffer, K.W. Baldwin, K.W. West, D. Goldhaber-Gordon, and R. de Picciotto, “Observation of a one-dimensional spin-orbit gap in a quantum wire,” *Nature Physics* **6**, 336 – 9 (2010).
 - [14] Jason Alicea, “Majorana fermions in a tunable semiconductor device,” *Phys. Rev. B* **81**, 125318 (2010).
 - [15] Roman M. Lutchyn, Tudor Stanescu, and S. Das Sarma, “Search for Majorana fermions in multiband semiconducting nanowires,” *Phys. Rev. Lett.* **106**, 127001 (2011).
 - [16] Tudor Stanescu, Roman M. Lutchyn, and S. Das Sarma, “Majorana fermions in semiconductor nanowires,” *Phys. Rev. B* **84**, 144522 (2011).
 - [17] K. Sengupta, Igor Žutić, Hyok-Jon Kwon, Victor M. Yakovenko, and S. Das Sarma, “Midgap edge states and pairing symmetry of quasi-one-dimensional organic superconductors,” *Phys. Rev. B* **63**, 144531 (2001).
 - [18] K. T. Law, Patrick A. Lee, and T. K. Ng, “Majorana fermion induced resonant Andreev reflection,” *Phys. Rev. Lett.* **103**, 237001 (2009).
 - [19] Jay D. Sau, Sumanta Tewari, Roman Lutchyn, Tudor Stanescu, and S. Das Sarma, “Non-abelian quantum order in spin-orbit-coupled semiconductors: The search for topological Majorana particles in solid state systems,” *Phys. Rev. B* **82**, 214509 (2010).
 - [20] G. Koren, T. Kirzhner, E. Lahoud, K. B. Chashka, and A. Kanigel, “Proximity-induced superconductivity in topological $\text{Bi}_2\text{Te}_2\text{Se}$ and Bi_2Se_3 films: Robust zero-energy bound state possibly due to Majorana fermions,” *Phys. Rev. B* **84**, 224521 (2011).
 - [21] D. Goldhaber-Gordon, H. Shtrikman, D. Mahalu, D. Abusch-Magler, U. Meirav, and M. A. Kastner, “Kondo effect in a single-electron transistor,” *Nature (London)* **391**, 156 (1998).
 - [22] S. M. Cronenwett, H. J. Lynch, D. Goldhaber-Gordon, L. P. Kouwenhoven, C. M. Marcus, K. Hirose, N. S. Wingreen, and V. Umansky, “Low-temperature fate of the 0.7 structure in a point contact: a Kondo-like correlated state in an open system,” *Phys. Rev. Lett.* **88**, 226805 (2002).
 - [23] H.-J. Kwon, K. Sengupta, and V.M. Yakovenko, “Fractional ac Josephson effect in p- and d-wave superconductors,” *The European Physical Journal B* **37**, 349–361 (2003).
 - [24] Liang Fu and C. L. Kane, “Josephson current and noise at a superconductor/quantum-spin-hall-insulator/superconductor junction,” *Phys. Rev. B* **79**, 161408 (2009).
 - [25] Michael Tinkham, *Introduction to superconductivity* (McGraw-Hill, New York, 1996).
 - [26] John Clarke and Alex I. Braginski, eds., *The SQUID Handbook: Fundamentals and Technology of SQUIDs and SQUID Systems, Volume I* (Wiley-VCH Verlag GmbH, 2005).
 - [27] A.F. Andreev, “Thermal conductivity of the intermediate state of superconductors,” *Zhurnal Eksperimental’noi i Teoreticheskoi Fiziki* **46**, 1823 – 1828 (1964).
 - [28] Yong-Joo Doh, Jorden A. van Dam, Aarnoud L. Roest, Erik P. A. M. Bakkers, Leo P. Kouwenhoven, and Silvano De Franceschi, “Tunable supercurrent through semiconductor nanowires,”

- Science **309**, 272–275 (2005).
- [29] Sidney Shapiro, “Josephson currents in superconducting tunneling: The effect of microwaves and other observations,” Phys. Rev. Lett. **11**, 80–82 (1963).
 - [30] J. D. Sau, S. Tewari, and S. Das Sarma, “Experimental and materials considerations for the topological superconducting state in electron and hole doped semiconductors: searching for non-Abelian Majorana modes in 1d nanowires and 2d heterostructures,” Phys. Rev. B **85**, 064512 (2012).
 - [31] K. K. Likharev, “Superconducting weak links,” Rev. Mod. Phys. **51**, 101–159 (1979).
 - [32] K. K. Likharev, *Dynamics of Josephson junctions and circuits* (Gordon and Breach Science Publishing, Paris, 1984).
 - [33] Jason Alicea, Yuval Oreg, Gil Refael, Felix von Oppen, and Matthew P. A. Fisher, “Non-Abelian statistics and topological quantum information processing in 1d wire networks,” Nat Phys **7**, 412–417 (2011).

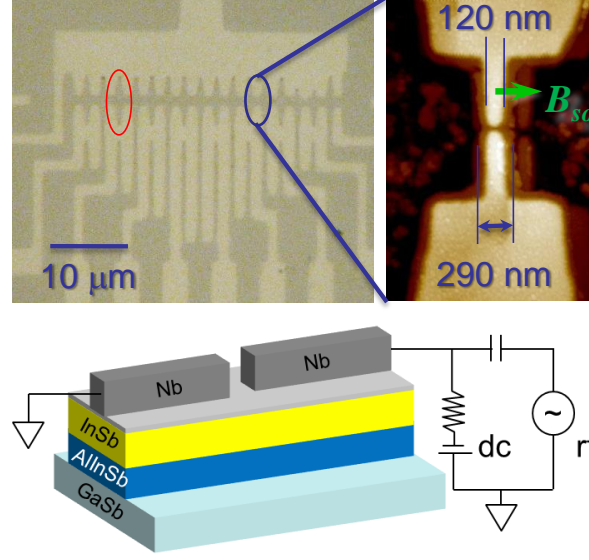


FIG. 1. Optical image of a sample with several dc SQUID devices. A single SQUID device is outlined with a red oval. On the AFM image a single Josephson junction is shown where the light areas are Nb. The shadow of the junction is a tip artifact. A light brown halo around Nb is a (thin 2-3 nm) Nb wetting layer which defines the width of the semiconductor wire after wet etching. The direction of the spin-orbit field B_{so} is indicated by the green arrow. The schematic at the bottom outlines the layer structure of the device.

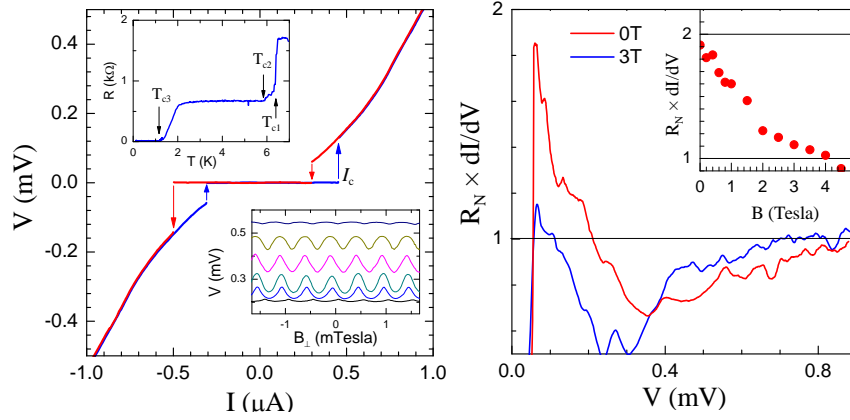


FIG. 2. A. A typical $V(I)$ characteristic of a Nb/InSb/Nb Josephson junction at 20 mK. In the top inset T -dependence of resistance shows three superconducting transitions $T_{c1} - T_{c3}$ for wide Nb areas, narrow Nb wires, and JJs, respectively. In the bottom inset dc SQUID operation of the device is plotted, measured at 300 mK. The different curves are for dc bias currents $I = 1.3 - 1.6 \mu\text{A}$ (bottom-to-top). B. Normalized differential conductance is plotted as a function of voltage across a JJ with $R_N = 650 \Omega$. At low V there is an enhancement of current, the signature of Andreev reflection. The maximum enhancement is plotted as a function of $\mathbf{B}||\mathbf{I}$ in the inset.

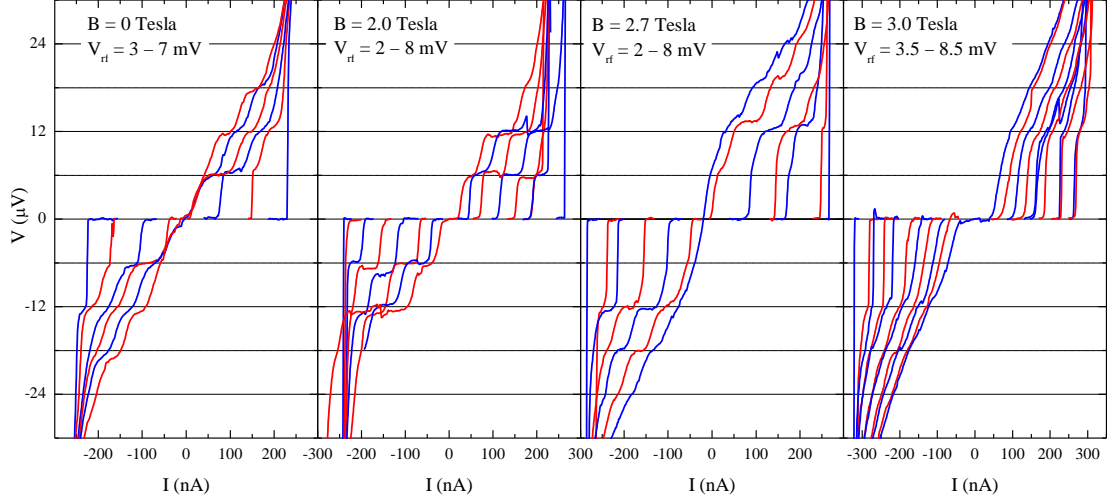


FIG. 3. $V(I)$ characteristics of a JJ in the presence of a $f_0 = 3$ GHz rf field of amplitude V_{rf} (at the top of the fridge) and $\mathbf{B} \parallel \mathbf{I}$. For $B < 2.5$ T Shapiro steps with Height $\Delta V = h\nu_{rf}/2e = 6 \mu\text{V}$ are observed. For $B > 2.5$ T the step at $6 \mu\text{V}$ disappears and the first Shapiro step is at $12 \mu\text{V}$. We interpret the ΔV doubling as an indication that supercurrent is carried by charge- e Majorana particles.

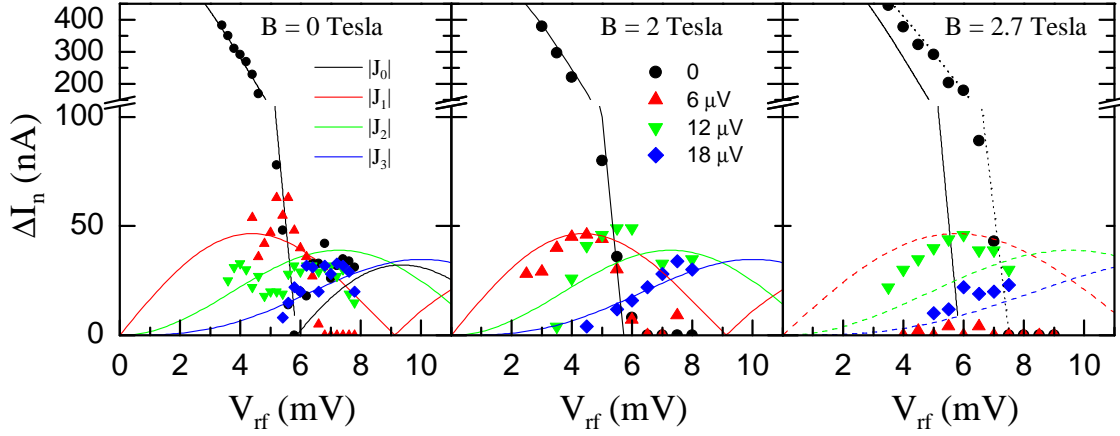


FIG. 4. Width of the first four Shapiro step ΔI_n plotted as a function of the rf field amplitude V_{rf} . Note that the scale of the vertical axis changes above the break. Lines are Bessel functions $A|J_n(\beta V_{rf})|$ with $\beta = 0.42 \text{ mV}^{-1}$ (solid) and $\beta = 0.32 \text{ mV}^{-1}$ (dashed). Amplitude A is 650 nA for $n = 0$ and $A = 80 \text{ nA}$ for $n = 1, 2$ and 3 . At 2.7 T step at $6 \mu\text{V}$ disappears, also step at $12 \mu\text{V}$ is better described by $|J_1|$ rather than by $|J_2|$ dependence. Doubling of the height of the Shapiro step is a signature of the fractional Josephson effect.

Supplementary Information

OBSERVATION OF THE FRACTIONAL JOSEPHSON EFFECT: THE SIGNATURE OF MAJORANA PARTICLES

Leonid P. Rokhinson, Xinyu Liu and Jacek K. Furdyna

I. ANALYSIS OF THE PARAMETER SPACE TO OBSERVE FRACTIONAL JOSEPHSON EFFECT

In order to form Majorana fermions in a nanowire several conditions have to be satisfied. The most stringent is lifting of the Kramers degeneracy, $E_Z > \sqrt{\Delta^2 + E_F^2}$, where E_Z is Zeeman energy $E_Z = g^* \mu_B B$, $g^* = 50$ for InSb, μ_B is Bohr magneton, and B is an external magnetic field. At the same time we need the proximity gap to be larger than the Josephson frequency, $\Delta > \hbar\omega_J = 6 \mu\text{eV}$ for 3 GHz, or $\Delta > 2\hbar\omega_J$ in the topological phase. The proximity gap Δ depends on the semiconductor-superconductor coupling λ , Zeeman energy and spin-orbit coupling [30]:

$$\Delta = \Delta_s \frac{\lambda}{\lambda + \Delta_s} \frac{E_{SO}}{\sqrt{E_{SO}^2 + E_Z^2}}. \quad (\text{S1})$$

The maximum Δ cannot exceed the superconducting gap in narrow Nb wires, $\Delta_s^w = 290 \mu\text{eV}$ for $T_c^w = 2 \text{ K}$, and is maximized for large coupling $\lambda \gtrsim \Delta_s$. Large coupling, though, increases electron density in the semiconductor which, in turn, increases E_F , thus requiring large fields to lift the Kramers degeneracy.

Let's analyze the parameters of the JJ8 device. We measured $T_c = 1.17 \text{ K}$, thus $\Delta = 1.76 k_B T / e = 180 \mu\text{eV}$ and $\lambda = 470 \mu\text{eV}$, or $\lambda \approx 2.6\Delta$. In our sample geometry we cannot measure electron density independently, but we can assume that at $B = 2 \text{ Tesla}$ (observed

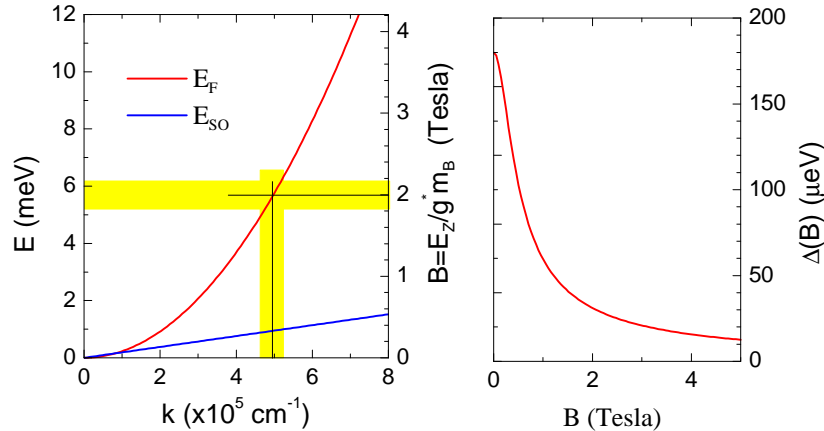


FIG. S5. Left: Fermi energy E_F and energy of spin-orbital coupling E_{SO} (for 20 nm InSb quantum well) are plotted as a function of carrier momentum k . The right axis show magnetic fields which correspond to the Zeeman energy of the left axis. Right: field dependence of the proximity gap for $E_{SO} = 1 \text{ meV}$.

topological phase transition) $E_Z = E_F$. We plot $E_F = 0.245k^2$ and $E_{SO} = \gamma_D \langle k_z^2 \rangle k = 0.19k$ as a function of $k[10^5 \text{ cm}^{-1}]$ in Fig. S5. We used $\gamma_D = 760 \text{ eV} \cdot \text{\AA}^3$, $\langle k_z^2 \rangle = (\pi/d)^2$, effective mass $m^* = 0.015$, and the quantum well thickness $d = 20 \text{ nm}$. At $B = 2 \text{ T}$ ($E_Z = 5.7 \text{ meV}$) the condition $E_F = E_Z$ translates into $k \approx 5 \cdot 10^5 \text{ cm}^{-1}$. Spin-orbit coupling for this k is estimated $E_{SO} \approx 1 \text{ meV}$. Expected field dependence of the proximity gap $\Delta(B)$ is plotted on the right plot for $E_{SO} = 1 \text{ meV}$. We see that at $B = 2 \text{ T}$ $\Delta = 30 \mu\text{eV}$ and the condition $\Delta > 2\hbar\omega_J$ is satisfied.

We observe Shapiro steps up to $\approx 3 \text{ T}$, which is consistent with the theoretically expected gap to be only $20 \mu\text{eV}$ at that field. Experimentally we measure slower I_c vs B dependence than the one predicted for Δ , Eq. (S1), see Section III.

The lithographical wire width is 290nm (the width of the Nb wire plus the wetting layer), and we expect the actual InSb wire width to be reduced due to etching and surface depletion. For an InSb wire with $100\text{-}250 \text{ nm}$ width the energy separation is in the $1.3\text{-}8 \text{ meV}$ range and only a few subbands are occupied for $E_F = 6 \text{ meV}$. **Thus, we conclude that experimental parameters for the JJ8 device satisfy the requirements for the observation of Majorana fermions.** We also note that high electron density and correspondingly large E_F in our wires helps to compensate the disorder introduced during the device fabrication.

II. PROXIMITY EFFECT IN INSB NANOWIRES

In order to verify that we observe a proximity-induced superconductivity we fabricated several (> 10) test devices on a semi-insulating GaAs substrate with the Nb pattern identical to the JJ devices, see inset in Fig. S6. Continuous wires show expected superconducting phase transitions at $T_{c1} = 7.5 \text{ K}$ for wide regions, $T_{c2} = 7.1 \text{ K}$ for $1 \mu\text{m}$ wide connectors and $T_{c3} = 1.9 \text{ K}$ for the 80 nm -wide wire. There is a 4 nm thick wetting layer around Nb, which can be seen as a halo around wires on the micrographs. For wires with small gaps $< 100 \text{ nm}$ the wetting layer fills the gap. The wetting layer is not attacked by the etching solution and serves as an etch mask in the semiconductor wire definition. In the device shown in Fig. S6 the gap is $\approx 40\text{nm}$. Yet these devices become insulating when cooled to low temperatures. This test experiment allows us to establish that (i) wetting layer is not conducting and plays no role in the electrical transport, (ii) tunneling current for gaps $> 20 \text{ nm}$ is negligible, and (iii) in InSb JJs current has to flow through the InSb layer. **Thus the observed superconductivity in InSb JJs is due to the proximity effect.**

III. TEMPERATURE DEPENDENCE OF JJ

Proximity-induced superconductivity has a reduced gap Δ compared to the gap of the host superconductor Eq. (S1), where λ is a semiconductor-superconductor coupling. The lowest T_c corresponds to this reduced proximity gap.

Temperature dependence of samples resistance is shown in Fig. S7. For a continuous line (L) we can identify three transition temperatures: $T_{C1} = 6.3 \text{ K}$ is for wide regions, $T_{C2} = 5.7 \text{ K}$ is for $1 \mu\text{m}$ -wide wires and $T_{C3} = 1.9 \text{ K}$ is for the 150 nm -wide wire. Similar results are obtained for Nb on GaAs, see the answer to Q8. Devices with a Josephson junctions (JJ6-8) have the actual superconducting transition $0 < T_C < T_{C3}$ for various devices. Note that in a ^3He , where electrical noises are higher, we do not observe superconducting transition for

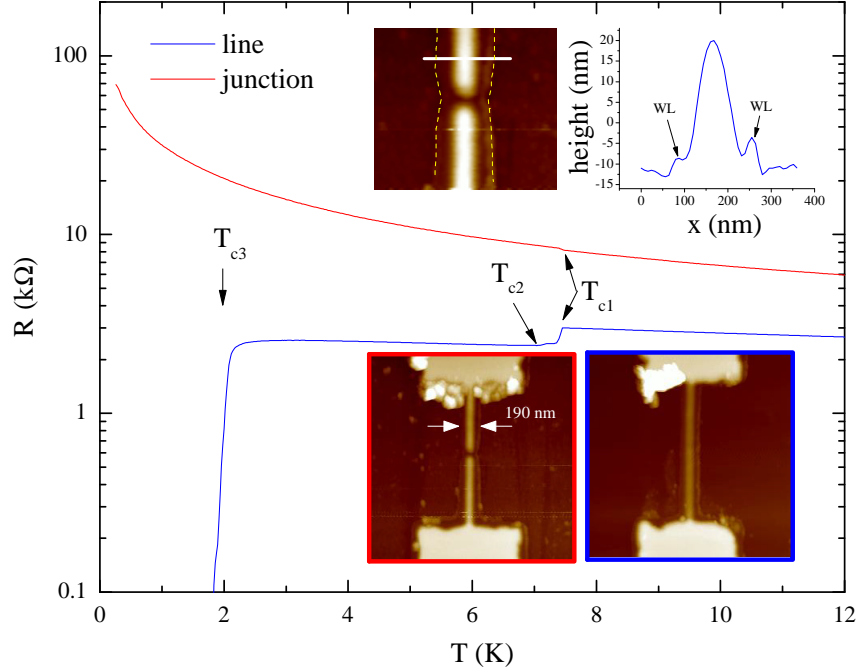


FIG. S6. Temperature dependence of a Nb junction and a continuous wire fabricated on a semi-insulating GaAs substrate. The wires are fabricated identically to the JJ on InSb substrates. In the bottom inset AFM micrographs of the junction and the wire devices are shown ($2\ \mu\text{m} \times 2\ \mu\text{m}$ scan size). On the top image a zoom of the gap region is shown. A 4 nm-high wetting layer around the wire and within the gap is clearly seen and is outlined with a dashed yellow line. The wire profile along the white line is shown on the right, and wetting layer (WL) is marked.

the JJ8 device down to 250 mK, the actual T_C for this device is 1.17 K, see inset.

IV. MAGNETIC FIELD DEPENDENCE OF CRITICAL CURRENT

The requirement is that the proximity gap $\Delta > k_B T, \hbar \omega_J$ in the semiconductor material at the fields we need to reach in order to satisfy the condition $E_Z > E_F$. In our Nb wires superconductivity survives up to 5 Tesla, see Fig. S8. In the low field region $I_c(B) \approx I_c(0)/\sqrt{1 - (B/B_1)^2}$ with $B_1 \approx 2.5$ T. Resistivity of crystalline Nb is $152\ \text{n}\Omega\cdot\text{m}$ and a perfect $L = 1.2\ \mu\text{m}$, $w = 100\ \text{nm}$ and $t = 40\ \text{nm}$ wire should have resistance of $\approx 1\ \Omega$. Our wires have resistance of $2\text{--}3\ \text{k}\Omega$, which indicates a substantial degree of disorder (at the same time our film $T_C \approx 7\ \text{K}$ is close to the bulk $T_c = 9.2\ \text{K}$). Disordered Nb is a type II superconductor and superconducting gap survives to much higher field $B_2 \approx 5\ \text{T}$. The thickness of the film $t = 40\ \text{nm}$ is of the order of the coherence length in Nb ($39\ \text{nm}$), thus flux capturing is possible even for the in-plane field.

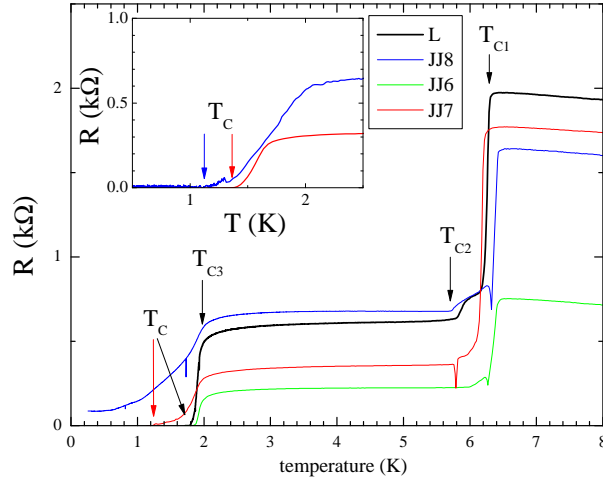


FIG. S7. Temperature dependence of resistance for the devices JJ6 (20 nm gap), JJ7 (30 nm gap), JJ8 (40 nm gap) and a continuous 150 nm-wide line (L) is measured in ^3He system (main plot) and in a dilution refrigerator (inset). The dilution refrigerator is properly shielded.

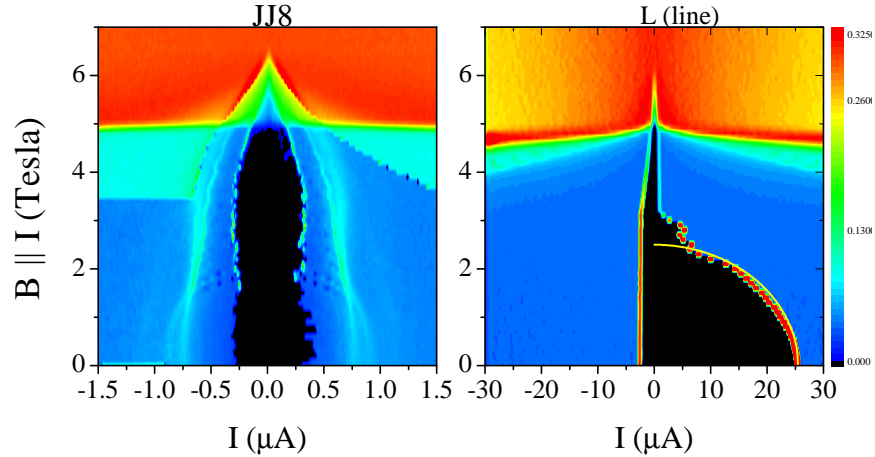


FIG. S8. Magnetic field dependence of differential resistance for device JJ8 and a 150 nm wide line fabricated next to it (L). Black regions are the superconducting states. Yellow line is $I_c/\sqrt{1 - (B/B_1)^2}$, where $B_1 = 2.5$ T is the first critical field.

V. FREQUENCY DEPENDENCE OF SHAPIRO STEPS

In Fig. S9 we show $V(I)$ traces measured in the presence of rf field with frequencies $f_0 = 2, 3$ and 4 GHz. The corresponding step heights are, respectively, $\Delta V = hf_0/2e = 4, 6$ and 8 μV .

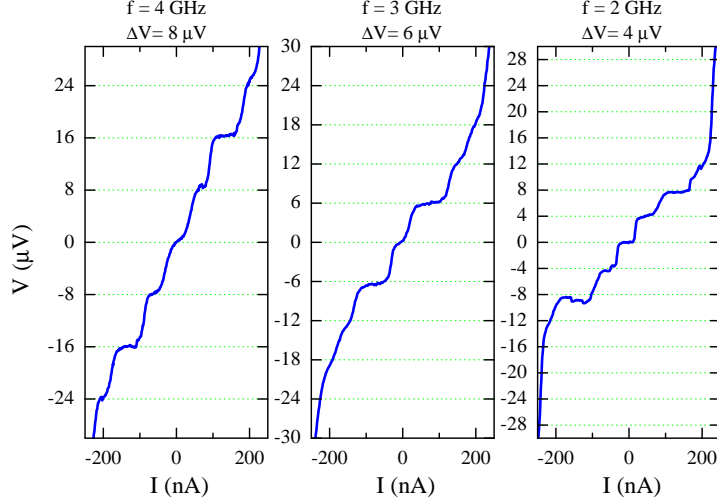


FIG. S9. Shapiro steps for rf frequencies $f_0 = 2, 3$ and 4 GHz.

VI. ANALYSIS OF THE JOSEPHSON JUNCTION

The $R_N = 650 \, \Omega$ quoted in the manuscript is the overall resistance of the device but not of the JJ, the difference is due to a low shunting resistance from the heavily doped substrate (the device-substrate resistance is $\approx 1 \, \text{k}\Omega$). The actual R_N for the JJ device can be estimated as follows. Next to the JJ8 device there is a $150 \, \text{nm}$ wide line with $R = 603 \, \Omega$ in the normal state. This resistance is the sum of the normal resistance of the wire and of the shunting resistance from the substrate, $R^{-1} = R_N^{-1} + R_s^{-1}$. A similar wire on an insulating substrate has $R_N = 2.5 \, \text{k}\Omega$, thus $R_s \approx 0.8 \, \text{k}\Omega$. Assuming that shunting resistance of the JJ8 and of the line are similar (the leakage to the substrate is primarily through contact pads of the same size) we estimate $R_N \approx 3 \, \text{k}\Omega$. The JJ8 device consists of two nominally identical JJs in parallel and the actual R_N for a single JJ can be as high as $\approx 6 \, \text{k}\Omega$. Thus, JJ8 has a few (< 10) subbands, which is also consistent with the number of subbands estimated from the size quantization, see Section I.

For short weak links in the dirty regime ($L_{eff} \ll \xi$ and $l \ll L_{eff}$, where l is the mean free path, ξ is the coherence length, and L_{eff} is the effective length of the weak link), the product $I_c R_N [\mu\text{V}] \approx 320 T_c [\text{K}]$ [31]. For the clean regime ($L_{eff} \ll l, \xi$) the value should be almost twice larger, $I_c R_N [\mu\text{V}] \approx 480 T_c [\text{K}]$. From the above estimates the product $I_c R_N \approx 900 \, \mu\text{V}$, while $T_c = 1.2 \, \text{K}$. Thus, JJ8 is in the clean regime, which is favorable for the observation of Majorana fermions.

VII. ANALYSIS OF SHAPIRO STEPS AS A FUNCTION OF RF POWER

In Fig. S10 we plot differential resistance $dV/dI(I, V_{rf})$ at $B = 0$ for the JJ8 device. Shapiro steps with $\Delta V = 6 \, \mu\text{V}$ are clearly seen at $V_{rf} > 2 \, \text{mV}$ and correspond to the black regions on the dV/dI contour plot. At high $V_{rf} > 4 \, \text{mV}$ evolution of the width of the Shapiro steps ΔI_n follows the Bessel functions pattern as a function of power, $\Delta I_n = A |J_n(2ev_{rf}/hf_0)|$, where v_{rf} is the rf amplitude on the junction and f_0 is the rf frequency. We can estimate the rf power attenuation from the second zero of the J_0 , $v_{rf} = 5.4 \cdot 10^{-3} V_{rf}$

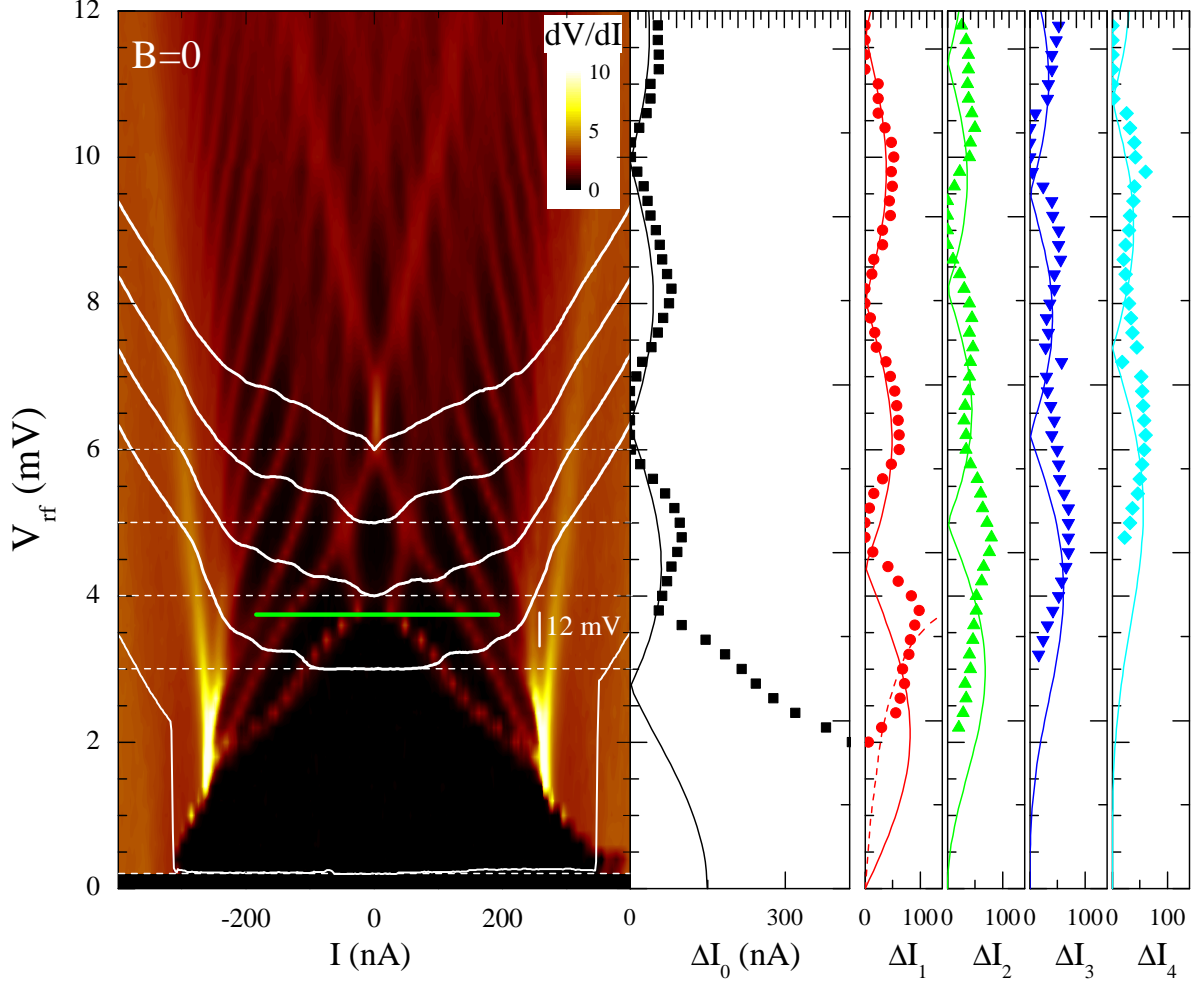


FIG. S10. Left: differential resistance dV/dI of the JJ8 is plotted as a function of the rf amplitude V_{rf} and dc current I . The rf frequency is $f_0 = 3$ GHz. The data is measured with low frequency (17 Hz) ac excitation $I_{ac} = 2$ nA at $T = 20$ mK and $B = 0$. $|V(I)|$ characteristics at $V_{rf} = 0.2, 3, 4, 5$ & 6 mV are shown as white lines, their zero is shifted vertically and is marked by dashed white lines. A small vertical bar is a $12 \mu\text{V}$ scale. Right: n -th step width ΔI_n is extracted from the dV/dI data and plotted as a function of V_{rf} for $n = 0 - 4$. Solid lines are Bessel functions $A|J_n(\beta V_{rf})|$ with $A = 150$ nA and $\beta = 0.89 \text{ mV}^{-1}$. A red dashed line for $n = 1$ is $\propto V_{rf}/\bar{I}$.

at $f_0 = 3$ GHz and $v_{rf} = 1.7 \cdot 10^{-3} V_{rf}$ at $f_0 = 4$ GHz. Here V_{rf} is the rf amplitude at the top of the fridge.

In the $dV/dI(I, V_{rf})$ plot we can identify two regions with different $\Delta I_0(V_{rf})$ dependencies, separated schematically by a green line at $V_{rf}^{crit} \approx 3.7$ mV. For the JJ8 device $V_c = I_R R_N \approx 65 \mu\text{eV} \ll \hbar f_0 / 2e = 6 \mu\text{eV}$, see Fig. S12, and for $V_{rf} < V_{rf}^{crit}$ the junction is in the small microwave signal regime [32]. The linear response of a JJ has a singularity at $\omega = \pm \omega_J$, and the first Shapiro step appears due to the phase locking of the external frequency and the Josephson oscillations. The JJ8 is in the intermediate dumping (resistively shunted) regime and the $V(I)$ characteristic is expected to become non-hysteretic in the vicinity of the first step. Indeed, we do not observe hysteresis for $V_{rf} > 1.8$ mV. **While nonlinear effects can**

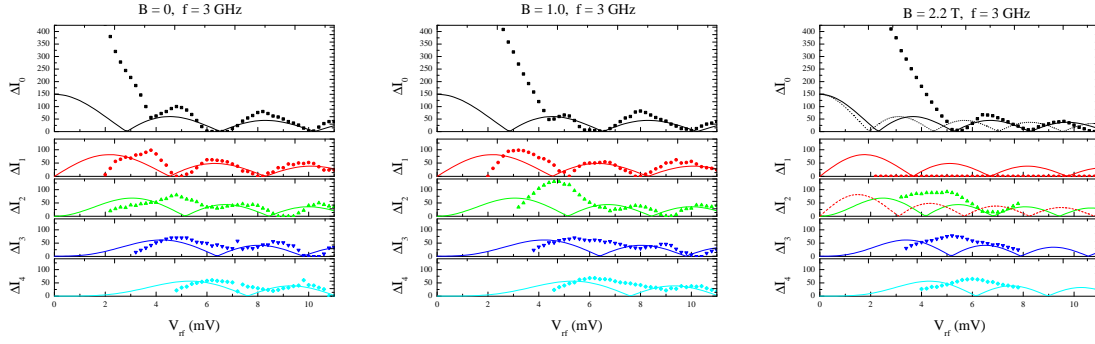


FIG. S11. Step width as a function of rf voltage amplitude V_{rf} is extracted from the data in Fig. S10 ($B = 0$) and similar data at 1.0 and 2.2 Tesla. Solid line are the Bessel functions.

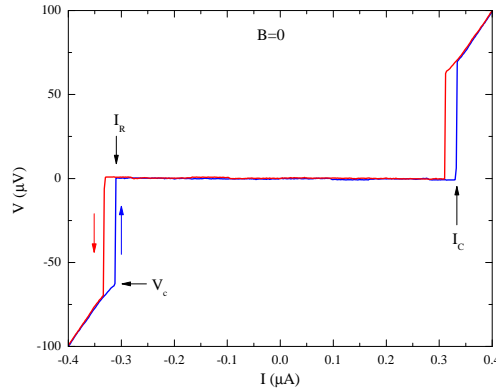


FIG. S12. Josephson junction JJ8 has small hysteresis at $B = 0$, $V_{rf} = 0$ and at $T = 20$ mK, which classifies it to be in an intermediate damping regime. The voltage $V_c \approx 65 \mu\text{eV}$ at the return critical current I_R is marked on the plot.

be present at high I and V_{rf} we want to stress that the first step at the onset of the normal state is due to the phase locking between the external and the Josephson frequencies, $\omega = \pm\omega_J$.

The width of the first step in the low rf power regime is expected to be $\Delta I_1 = 2I_c I_\omega / \bar{I}$, see dashed red line on $\Delta I_1(V_{rf})$ plot. At high power the width of the n -th step is expected to follow the n -th Bessel function. Indeed the step widths follow the expected pattern, some deviations are expected due the sample being in a crossover regime between the low and high power regimes.

VIII. MAGNETIC FIELD DEPENDENCE OF THE SHAPIRO STEPS

A detailed field dependence of the steps evolution is given in Fig. S13 and analysis of step width as a function of rf power is discussed in Section VII. We note that for the first cooldown the $6 \mu\text{V}$ step was observed up to ≈ 2.5 Tesla (data in Figs 3, 4), while in a subsequent

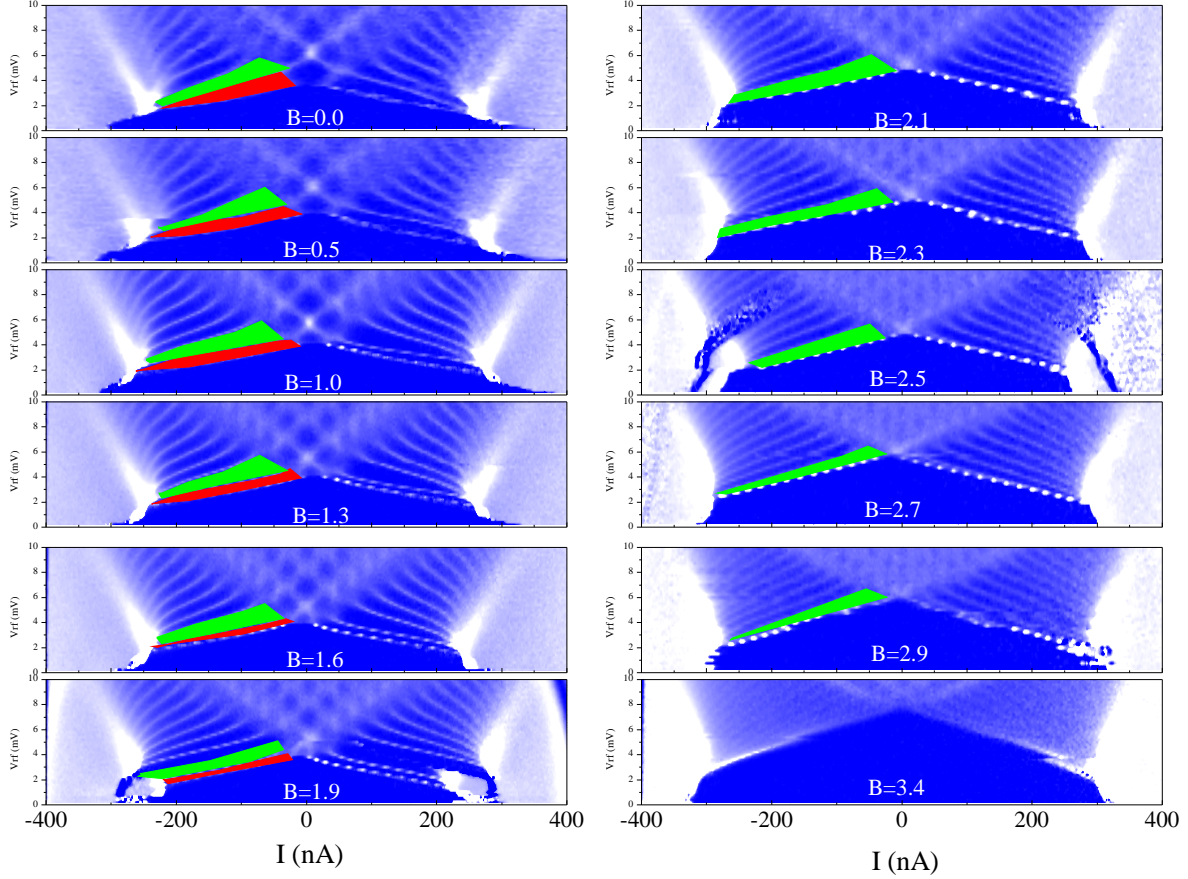


FIG. S13. Evolution of Shapiro steps in JJ8 with magnetic field. The data is measured with $I_{ac} = 2$ nA at $T = 20$ mK. The steps at $6 \mu\text{V}$ and $12 \mu\text{V}$ are outlined with red and green, respectively, we used $V(I)$ data to identify the step height. Note that the $6 \mu\text{V}$ step disappears for $B > 2$ Tesla.

cooldown the transition shifted to ≈ 2 Tesla. The shift of the transition temperature is most likely due to the lowering of the electron density in the InSb nanowire due to side wall oxidation of InSb after prolonged exposure to the air. When electron density is reduced, the condition $E_F < E_Z$ is satisfied at lower B .

IX. DISCUSSION OF THE RELATION BETWEEN 2π AND 4π PERIODICITY AT HIGH FIELDS

It has been argued that both 2π and 4π periodicity should be present in the topological state, yet the 2π periodicity is suppressed by a factor of Γ/Δ , see [33]:

$$I = \frac{e\Gamma}{2\hbar} \sin(\phi/2) - \frac{3e\Gamma^2}{16t\hbar} \sin(\phi/2),$$

where tunneling $t = \Delta$ in the model, and Γ is the coupling between end Majorana states across the junction. In essence, Cooper pairing is still allowed but Cooper pairs are displaced away from the junction by the Andreev bound states, which reduces tunneling.

Qualitatively, we expect Γ to increase at higher voltages and Cooper pair contribution to the supercurrent to become more important. We do not see the first plateau at high fields, which means that Cooper pair tunneling is negligible at small voltages in our experiments. It may already contribute to the width of the second plateau but we cannot separate the two additive components with the same frequency. The increase of Γ with V and enhanced Cooper pair contribution to the Josephson current qualitatively explains the prominence of the 18 μV and higher plateaus even at high fields.